ASTRONOMY & ASTROPHYSICS
SUPPLEMENT SERIES

Astron. Astrophys. Suppl. Ser. **129,** 191-194 (1998)

On the effect of narrow-band filters on the diffraction limited resolution of astronomical telescopes

J.M. Beckers

National Solar Observatory, Tucson, AZ 85726/Sunspot, NM 88349, U.S.A.

Received August 27; accepted September 4, 1997

Abstract. Sometimes Fabry-Perot and other narrow-band filters are used for astronomical imaging in the so-called telecentric mode. In it the pupil is collimated through the filter, resulting in different incidence angles on the filter for rays coming from different parts of the objective. This results in variations of the central transmission wavelength, which broaden the effective filter bandpath. In addition each wavelength within this filter bandpath sees a different illumination of the pupil when viewed from behind the filter. This causes the diffraction limited point-spread-function to vary with wavelength. With the advent of diffraction limited imaging using adaptive optics, this can cause complications. In this note I examine the magnitude of this effect.

Key words: instrumentation: interferometers — instrumentation: spectrographs — techniques: interferometric

1. Introduction

Narrow band filters used for astronomical imaging have relatively small acceptance angles. As the optical rays deviate from normal incidence (incidence angle $\theta = 0°$), the wavelength λ of the filter shifts. For Fabry-Perot filters and etalons the relative shift $\Delta\lambda/\lambda$ equals $\theta^2/2\mu$ for small angles θ and for a refractive index in the filter cavity of μ. To avoid broadening of the bandpath, filters are therefore mostly used in an optical configuration where the sky image is collimated through the filter. The drawback of that is that the wavelength varies across the field of view, an effect that has to be taken into account when analyzing the observations. This is, for example, the case for the TAURUS narrow band imaging interferometer in use at a number of observatories (see Taylor & Atherton 1980 and Atherton et al. 1982).

Send offprint requests to: J.M. Beckers

In order to avoid this variation of wavelength across the field-of-view, Bonaccini et al. (1989) and Cavallini (1997) use a Fabry-Perot etalon in the so-called telecentric mode in which the telescope objective is collimated through the filter. This has two side effects: (i) it broadens the filter bandpath (in the Cavallini instrument from ~ 0.8 pm to ~ 2 pm; 1 pm being 10 mÅ), and (ii) it affects the imaging quality of the telescope in case of diffraction limited imaging because of uneven illumination of the pupil when viewed from behind the etalon, an effect which varies with wavelength. The former effect was recognized by the authors, who in fact have used it to their advantage to broaden the filter bandpath to the desired 2 pm value. The latter effect has not been evaluated anywhere to my knowledge. It is of special interest in an era where the implementation of adaptive optics at many telescopes is sought in order to achieve diffraction limited images. Its assessment is the subject of this paper.

2. Input parameters

The transmission $\tau(\lambda)$ and the peak transmission wavelengths λ_0 of a Fabry-Perot etalon equals:

$$\tau(\lambda) = T^2(1-R)^{-2}\left[1 + 4R(1-R)^{-2}\sin^2(2\pi\mu t\cos\theta/\lambda)\right]^{-1} \quad (1)$$

and

$$\lambda_0 = 2\mu t\cos\theta/N \quad (2)$$

(Atherton 1987), where T and R are the transmission and reflection coefficients of each surface, t is the Fabry-Perot cavity spacing and N is the interference order.

Except where mentioned differently, I will assume the values given by Cavallini (1998) for a Queensgate Fabry-Perot etalon: $R = 0.95$, $\lambda = 550$ nm, $t = 3$ mm, $\mu = 1.0$ and a telecentric beam with an f-ratio of $f/192$. I will assume in this note perfect optical quality for the Fabry-Perot plates and a normal incidence angle of the central ray on the etalon. With these parameters N equals 10909 and the Fabry-Perot FWHM in collimated light 0.823 pm. The wavelength shift across the pupil equals 1.865 pm.

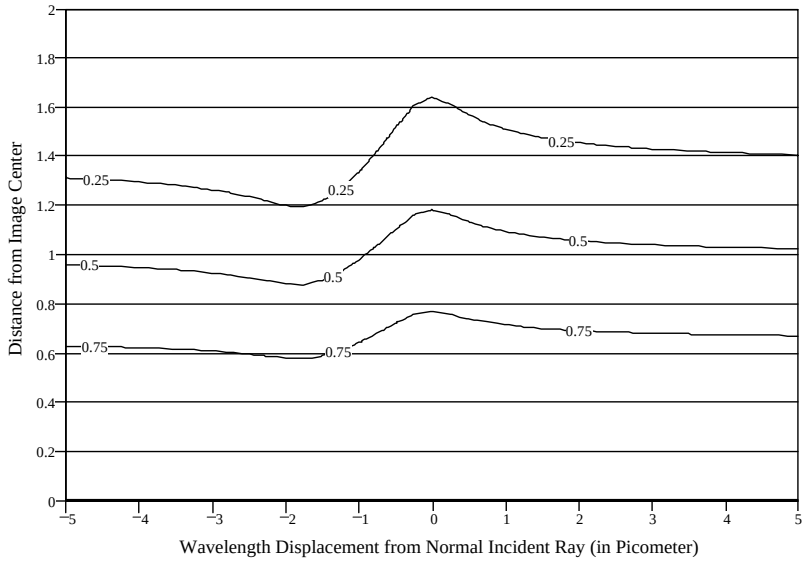

Fig. 1. Point-spread-function shape as a function of wavelength. Shown are the PSF widths for three fractions of the peak intensity in units of the FWHM of the Airy function

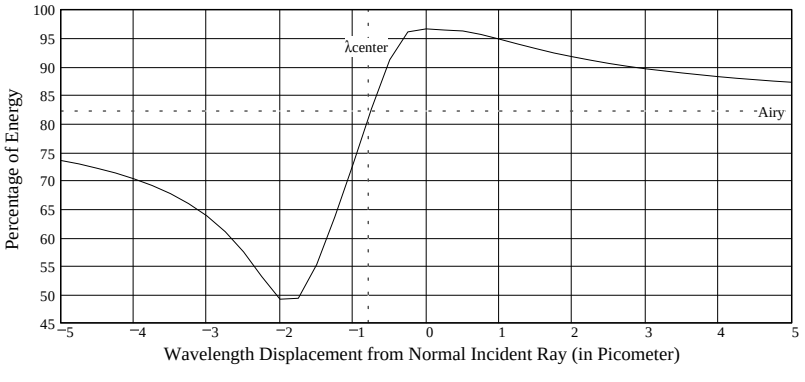

Fig. 2. Percentage of energy of the PSF contained in the image area within the first dark Airy ring of a uniform illuminated aperture. $\lambda_{\mathrm{center}}$ is the wavelength of peak the total filter transmission

Table 1. Properties of Fabry-Perot interferometer in telecentric configuration for different f-ratios

f-Ratio	**Maximum λ Shift (pm)**	**Spectral FWHM (pm)**	**Line Shift (pm)**	**Minimum Energy** E_{min}	**Maximum Energy** E_{max}
$f/150$	3.06	2.92	-1.18	38%	96%
$f/192$	1.86	1.90	-0.79	49%	97%
$f/200$	1.72	1.78	-0.74	50%	97%
$f/250$	1.10	1.30	-0.49	59%	96%
$f/350$	0.56	0.96	-0.26	69%	92%
$f/500$	0.28	0.90	-0.13	76%	88%
$f/1000$	0.07	0.83	-0.02	81%	84%
f/∞	0.00	0.82	0.00	82%	82%

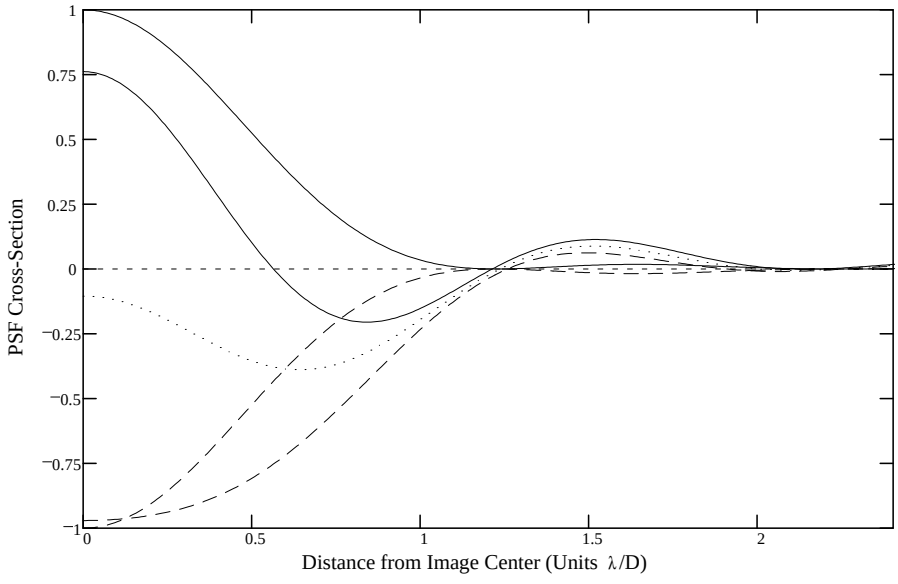

Fig. 3. Point-spread-functions in velocity images for Doppler shifts corresponding to +100 m/s (full drawn line), −100 m/s (dashed line) and 0 m/s (dotted line). The heavy lines correspond to the full telecentric configuration, the thin line to the (artificially) uniform illuminated pupil

3. Calculations

At a wavelength displacement of $\Delta\lambda$ from λ_0 the illumination of the pupil in monochromatic light equals:

$$I(\alpha,\ \beta) = I_0 \left[1 + 4R(1-R)^{-2} \sin^2(2\pi\mu t \cos\theta/(\lambda_0 - \Delta\lambda)\right]^{-1} \quad (3)$$

where α and β are orthogonal coordinates in the pupil and $\alpha^2 + \beta^2 = \theta^2$. The wave amplitude $A(\alpha, \beta)$ equals $I^{0.5}(\alpha,\ \beta)$.

The amplitude distribution in the image plane is the Fourier transform $\tilde{A}$ of $A(\alpha,\ \beta)$, and the image point-spread-function (PSF) intensity is $\tilde{A}^2$.

4. Results

Figure 1 shows the width of the PSF as a function of wavelength displacement for the on-axis ray on the Fabry Perot centered on a wavelength displacement of 0 pm for the 75, 50 and 25 percentile peak values, the 50 percentile value corresponding to the full width at half maximum (FWHM). All values are normalized to the FWHM of an evenly illuminated pupil (the Airy disk) which corresponds to $1.019\lambda/D$ where D is the telescope diameter. At displacements towards the blue the PSF narrows because of the increase in illumination towards the edges of the pupil. The opposite is the case for red wavelength displacements. The effects of the uneven illumination of the pupil caused by the telecentric configuration of the rays through the Fabry-Perot is considerable. Figure 2 gives a different evaluation of the PSF. It shows the amount of energy E contained within the first dark Airy ring of the same telescope but with uniform aperture illumination (radius $1.22\lambda/D$). For an Airy disk the amount equals 82%. In the telecentric Fabry-Perot it ranges between $E_{\min} = 49\%$ in the blue wing of the filter profile to $E_{\max} = 97\%$ in the red wing. Table 1 lists the properties of the telecentric Fabry-Perot profile and PSF behavior with different f-ratios of the telecentric beam. Obviously the slower the f-ratio, the smaller the PSF effects.

The effect on the astronomical observations is, of course, dependent on the actual observational configuration used. Solar spectral lines have a typical width of 10 pm so that Doppler shift observations require two observations with the filter transmission shifted by approximately 5 pm to either sides of the line center. The diffraction limited PSF in the red wing will be broader than that in the blue wing which will give rise to artificial velocity signals.

To assess the magnitude of the effect, I calculated the velocity image which would be seen for a velocity point on the solar surface if it were obtained by subtraction of two intensity images taken in the blue and red wing of a Gaussian shaped absorption line at 550 nm wavelength, with a central intensity of 33.33% of the continuum intensity and a FWHM of 10 pm. Such a line is similar in properties to the often used 617.3 and 630.3 nm Fraunhofer lines. The images were taken at ±5 pm from line center, where line center was chosen such that the spatially and spectrally integrated intensities were equal in the two wings. Figure 3 shows cross-sections through the resulting velocity image PSFs for Doppler velocities of 0 and

±100 m/s. Also shown, on the same relative intensity scale, are the cross-sections for the case of a uniform pupil illumination as seen from behind the etalon (but assuming the same telecentric spectral transmission profile). One notices: (i) the fully artificial velocity signal in case of zero Doppler shift. Its amplitude equals approximately that of a real 30 m/s feature observed in the collimated configuration. For a uniform solar image without velocity structure this artificial signal, of course, averages out. But for an image with surface structure it doesn't, and (ii) the very different PSFs for up- and downward motions, different both in the image core and in the far wings.

5. Conclusion

It is obvious that collimated imaging through Fabry-Perot filters is to be preferred when diffraction limited imaging is attempted. The advantages of telecentric imaging (uniform spectral transmission across the field-of-view) are then not longer possible. In case of the use of adaptive optics for diffraction limited imaging, the isoplanatic patch, however, limits the field-of-view to only a few arcsec anyway, so that the variation of the filter transmission across the field-of-view is minor.

References

Atherton P., 1987, in: Instrumentation for Ground-Based Optical Astronomy, Robinson L.B. (ed.). Berlin, Springer Verlag, p. 124

Atherton P.D., Taylor K., Pike C.D., Harmer C.F.W., Parker N.M., Hook R.N., 1982, MNRAS 202, 661

Bonaccini D., Cavallini F., Ceppatelli G., Righini A., 1989, A&A 217, 368

Cavallini F., 1997, A&A (in print)

Taylor K., Atherton P.D., 1980, MNRAS 191, 675